CME SAM

Cardiac MRI

AJR FOCUS ON:

Cardiac MRI: Part 2, Pericardial Diseases

Prabhakar Rajiah[1]

OBJECTIVE. MRI plays an important role in the morphologic and functional evaluation of pericardial diseases. MRI has the advantages of high spatiotemporal resolution, soft-tissue contrast, wide FOV, and multiplanar imaging capabilities, making it a valuable tool in the evaluation of pericardial disorders. In this article, the role of MRI in the evaluation of pericardial disorders, including pericardial constriction, is described and illustrated.

CONCLUSION. MRI is a vital diagnostic tool in the evaluation of pericardial diseases, particularly inflammation and constriction, because it can provide both morphologic and functional information essential for determining the optimal therapeutic strategy. It is used for the characterization and delineation of the extent of spread of pericardial masses. Various imaging sequences are available, so the MRI protocol should be optimized and tailored to the specific clinical condition that is being evaluated.

The pericardium is affected by various pathologic processes that result in variable clinical dysfunction [1]. Imaging modalities such as echocardiography, CT, and cardiac catheterization play a vital role in the diagnosis of these abnormalities, particularly when the clinical findings are equivocal. Echocardiography is often the first-line imaging modality because of its low cost, wide availability, and portability. However, echocardiography is challenging in the presence of limited windows, obesity, obstructive lung disease, chest wall deformities, and post surgical changes. In addition, it is highly operator dependent, has a narrow FOV, and has limited tissue characterization.

Cardiac CT has good spatial and temporal resolution, a wide FOV, and multiplanar reconstruction abilities. It is the ideal technique for the evaluation of pericardial calcification and is very useful in preoperative planning. However, CT may be associated with complications related to radiation and iodinated contrast medium. In addition, functional evaluation is limited unless a retrospective study is performed, which is associated with a higher radiation dose than conventional prospective ECG gated study. The newer CT scanners can perform retrospective ECG gated study with a dose lower than a typical dose of conventional chest CT. Imaging can be challenging in patients with arrhythmia or poor breath-holders and should be avoided in hemodynamically unstable patients. Cardiac catheterization is used for direct measurement of ventricular pressures [1].

MRI is a valuable imaging tool—in both the morphologic and the functional assessments—for evaluating pericardial abnormalities. MRI has the advantages of being noninvasive and not using radiation or potentially nephrotoxic iodinated contrast agents. In addition, it also has good spatial resolution, high inherent soft-tissue contrast, a wide FOV, and multiplanar imaging capabilities; these characteristics of MRI are useful in the evaluation of pericardium, particularly for tissue characterization, assessment of inflammation, and evaluation for other potential cardiac abnormalities. MRI is ideally suited for evaluation of small or loculated pericardial effusions, pericardial inflammation, and functional abnormalities caused by pericardial constriction and for characterization of pericardial masses. The wide FOV enables assessment of surrounding structures as well. However, MRI cannot be performed in patients with contraindications, claustrophobia, or severe renal dysfunction and is performed in hemodynamically stable patients only. Imaging can

Keywords: constriction, MRI, pericarditis, pericardium

DOI:10.2214/AJR.10.7265

Received April 26, 2010; accepted after revision December 27, 2010.

[1]Imaging Institute, Cleveland Clinic, 9500 Euclid Ave, Cleveland, OH 44195. Address correspondence to P. Rajiah (radprabhakar@gmail.com).

SAM/CME
This article is available for SAM/CME credit.
See www.arrs.org for more information.

WEB
This is a Web exclusive article.

AJR 2011; 197:W621–W634

0361–803X/11/1974–W621

be challenging in patients who cannot hold their breath or in those with severe arrhythmias who might require free-breathing techniques. MRI is not suitable for the detection of calcifications [2].

In this article, the MRI appearances of various pericardial diseases are discussed and illustrated. In addition, an MRI protocol for the evaluation of pericardial diseases is also described.

Pericardial Anatomy

The pericardium has an outer fibrous layer and an inner serous layer that envelop not only the heart, but also the proximal portions of the ascending aorta, pulmonary artery, left pulmonary veins, and superior vena cava (SVC). The fibrous layer is more distensible than the serous layer, although it is attached to the diaphragm, sternum, costal cartilages, and external layer of the great vessels [3]. The serous pericardium has an outer parietal layer and inner visceral layer. The parietal layer lines the inner surface of the fibrous pericardium to which it adheres, whereas the visceral layer envelops the epicardial surface of the heart, separated from it only by a layer of epicardial fat that contains the coronary vessels. The pericardial cavity is the space between the parietal and visceral pericardial layers that typically contains 15–50 mL of clear serous fluid produced by visceral pericardium, mostly plasma ultrafiltrate [4] and cardiac lymph, that eventually drains into the thoracic duct and right lymphatic ducts [2].

Pericardial Recesses and Sinuses

The pericardium has two main sinuses, the transverse and oblique, and multiple recesses. The transverse sinus is anterosuperior to the left atrium and separates an anterosuperior pericardial sleeve enclosing the aorta and pulmonary artery from a posterosuperior pericardial sleeve enclosing the SVC and pulmonary veins [2]. It has superior aortic, inferior aortic, and right and left pulmonary recesses. The superior aortic recess is divided into posterior, right lateral, and anterior components on the basis of its relationship to the ascending aorta. The transverse sinus is anterosuperior to the oblique sinus, which is posterior to the left atrium, and is separated from the left atrium by a reflection of pericardium between the right and left superior pulmonary veins [5–8]. The posterior wall of the left atrium is separated from the pericardial space; as a result, fluid collects in this area only if the effusion is large [2]. The posterior pericardial recess is the most cranial reflection of the oblique sinus. Pulmonary recesses are located between the superior and inferior pulmonary veins, and the postcaval recess is located posterior and to the right of the SVC [8]. Knowledge of these recesses and sinuses is essential to avoid misinterpreting these normal structures as lymph nodes, mediastinal masses, or dissection.

Pericardial Function

The pericardium serves various functions: It fixes the position of the heart within the mediastinum, decreases the friction of cardiac movements, and limits the spread of diseases to the heart from adjacent structures. Respiratory variations of intrathoracic pressure are transmitted to the pericardial cavity and subsequently to the cardiac chambers and are more pronounced on the thin-walled right ventricle. Atrial filling is supported by the negative systolic pericardial pressure. The pericardium limits acute cardiac chamber dilatation during diastole, particularly of the thin-walled right atrium and right ventricle, and prevents ventriculoatrial reflux when end-diastolic pressure is elevated. The pericardium plays an important role in the adaption of the right ventricular stroke volume to the left ventricular stroke volume when systemic vascular resistance is elevated and equalizing compliance between the thin-walled right and thick-walled left ventricles, resulting in interdependence of left and right ventricular filling (ventricular coupling) [2, 9].

MRI Protocol

A standard MRI protocol used at our institution for imaging the pericardium, which typically takes 30–40 minutes, is given in Table 1. Sequences can be added or removed depending on the disease process and patient condition (e.g., breath-holding capacity, arrhythmia, metal).

Scout Images

Scout images in the axial, coronal, and sagittal planes are used in the planning of subsequent cardiac views. In addition, sagittal images are used to confirm that the heart is positioned at the center of the coil.

TABLE 1: MRI Sequences and Planes Used to Evaluate the Pericardium

Sequence	Planes	Information
Scouts	Axial, sagittal, coronal	Localizing
HASTE FSE	Axial	Define anatomy and plan subsequent views
Cine SSFP	Vertical long-axis, horizontal long-axis, short-axis, four-chamber, LVOT	Evaluate function, volumes, masses
Myocardial tagging	LV short-axis × 3 (i.e., base, mid, distal), vertical long-axis, four-chamber, LVOT	Evaluate pericardial movement
T1 and T2 FSE	Vertical long-axis, short-axis, four-chamber, LVOT	Assess pericardial morphology
T2 FSE STIR	Vertical long-axis, short-axis, four-chamber, LVOT	Evaluate for pericardial edema due to inflammation
Velocity-encoded[a] phase-contrast	Mid ascending aorta	Assess aortic flow and flow pattern of SVC and pulmonary vein
Early contrast-enhanced T1-weighted FSE	Vertical long-axis, short-axis, four-chamber, LVOT	Evaluate for inflammation, masses
Delayed enhancement	vertical long-axis, short-axis, four-chamber, LVOT	Evaluate for pericardial inflammation and fibrosis, masses
Real-time imaging	Short axis, mid ventricle	Evaluate for ventricular interdependence

Note—FSE = fast spin-echo, SSFP = steady-state free precession, LVOT = left ventricular outflow tract, SPAMM = spatial modulation of magnetization, LV = left ventricular, SVC = superior vena cava.
[a]Velocity encoding = 200 cm/s.

Axial Fast Spin-Echo (FSE) Images

Half-Fourier acquisition single shot turbo spin echo (HASTE) images are acquired through the chest (TR/TE, 1500/30; flip angle, 160°; average number of slices, 16–20; slice thickness, 8.0 mm; gap, 0.8 mm). These are rapid acquisitions that do not require a breath-hold but are performed with ECG gating. These images can detect abnormalities in the lungs and mediastinum, including pleural effusion, ascites, and dilatation of veins. In addition, they are used to plan subsequent cardiac views.

Cine Steady-State Free Precession Imaging

Cine steady-state free precession (SSFP) images (TR/TE, 2.8/1.4; flip angle, 70°; slice thickness, 8 mm; gap, 2 mm; matrix, 240–360 × 300–380 mm) should be obtained in vertical long-axis, short-axis, four-chamber, and left ventricular outflow tract (LVOT) planes. Each image is typically acquired in one breath-hold. Tissues with a high T2/T1 ratio such as fluid, fat, and blood will appear bright in this sequence, but tissues with low T2/T1 such as myocardium appear dark to intermediate. This sequence is ideal for evaluating global and regional myocardial function, cardiac volumes, and cardiac masses. The functional consequences of pericardial constriction are best assessed in these views. In addition, abnormal diastolic filling can be quantified by assessing ventricular volumes over time.

Myocardial Tagging With Spatial Modulation of Magnetization

Myocardial tagging with spatial modulation of magnetization (SPAMM) (TR/TE, 4.2/1.9; flip angle, 15°; slice thickness, 8 mm; gap, 10 mm; matrix, 256 × 256 mm) should be performed in vertical long-axis, short-axis, four-chamber, and LVOT projections. Tags are seen as dark bands in the myocardium that fade over time. In healthy persons, the continuity of the tags is lost between the visceral and parietal pericardium during the cardiac cycle. However, this feature is altered in constriction, making this sequence useful in the detection of pericardial adhesion and myocardial involvement.

T2-Weighted Double-Inversion Fast Spin-Echo Imaging

T2-weighted double-inversion FSE images (TR/TE, 2000/80; TR, 2 or 3 R-R intervals; inversion time [TI], 150 ms; section thickness, 8 mm; gap, 2 mm; matrix, 256 × 256; echo-train length, 20–32) should be obtained in vertical long-axis, short-axis, four-chamber, and LVOT projections. In this sequence, the blood pool appears dark because of double inversion, but myocardium and pericardium have intermediate signal. This sequence is used for morphologic assessment of the pericardium, including evaluating for thickening, effusions, and masses.

T2-Weighted Triple-Inversion Fast Spin-Echo and STIR Imaging

T2-weighted triple-inversion FSE and STIR images (TR/TE, 2000/80; TR, 2 or 3 R-R intervals; TI, 150 ms; section thickness, 8 mm; gap, 2 mm, matrix, 256 × 256; echo-train length, 20–32) should be obtained in vertical long-axis, short-axis, four-chamber, and LVOT projections. These images are similar to T2-weighted FSE images but with additional fat suppression that enables detection of myocardial edema and pericardial fluid or edema.

T1-Weighted Fast Spin-Echo Imaging

T1-weighted FSE sequences should be performed approximately 15 seconds after IV injection of 0.1–0.2 mmol/kg of contrast material (TR/TE, 1000/25; TR, 1 R-R interval; section thickness, 8 mm; gap, 2 mm; matrix, 256 × 256) in vertical long-axis, short-axis, four-chamber, and LVOT projections. These images are used in the detection of pericardial contrast enhancement, which is a feature of acute and chronic inflammatory pericarditis. Contrast enhancement in pericardial tumors can also be assessed.

Delayed Enhancement Imaging

Inversion recovery delayed enhanced images are acquired 8–10 minutes after injection of 0.1–0.2 mmol/kg of gadolinium. Before this sequence, a "Look-Locker" sequence is acquired (TR/TE, 8/3; flip angle, 12°; 1 slice repeated 32 times; slice thickness, 10 mm) to identify the optimal inversion time. A segmented phase-sensitive inversion recovery gradient-echo sequence (TR/TE, 6.5/3.2; trigger pulse, 2; flip angle, 15°; average number of slices, 8–12; slice thickness, 8 mm; gap, 2 mm) is acquired in vertical long-axis, short-axis, four-chamber, and LVOT planes. This sequence enables detection of pericardial and myocardial inflammation and masses. Delayed enhancement imaging can also be performed using 2D, 3D, phase sensitive or single-shot inversion recovery techniques.

Velocity-Encoded Phase-Contrast Imaging

Velocity-encoded phase-contrast images (TR/TE, 5.0 /3.1; flip angle, 30°; slice thickness, 6 mm; matrix, 240–360 × 300–380 mm) are acquired at the level of the mid ascending aorta. This sequence enables quantification of flow in the aorta. In addition, analyses of flow and velocity patterns in the SVC and pulmonary veins at this same level enable estimations of the right and left atrial pressure curves.

Real-Time Cine Imaging

Real-time cine images (TR/TE, 2.3/1.1; flip angle, 50°; slice thickness, 10 mm; matrix, 85–100 × 128–150 mm) should be obtained in the short-axis plane. This sequence has low spatial resolution, but it has high temporal resolution that is useful in the assessment of rapid physiologic changes. This sequence enables detection of respiratory variation of the septal motion, which is very helpful in the diagnosis of pericardial constriction.

MRI of Normal Pericardium

At MRI, normal pericardium is seen as a smooth, curvilinear structure that is surrounded on either side by high-signal epicardial and mediastinal fat. Normal pericardium has intermediate-to-low signal on T1- and T2-weighted black blood FSE (Fig. 1) and SSFP sequences. The two pericardial layers are not separately discerned. The presence of fat and fluid makes visualization of pericardium easier. Although the pericardium is prominently seen adjacent to the right ventricular free wall, right atrioventricular groove, inferior aspect of the left ventricle, and left ventricular apex [10], it is visualized less clearly adjacent to the lateral left ventricular wall because of the paucity of fat and low signal from adjacent lungs [2]. Normal pericardium measures 0.4–1.0 mm thick in autopsy studies [11], but normal pericardium measures 1.2 mm in diastole and 1.7 mm in systole on MRI studies [2]. The higher thickness of normal pericardium on MRI results from a combination of cardiac motion, low spatial resolution with partial volume averaging, and chemical-shift artifact [2]. Normal pericardium does not have early or delayed contrast enhancement.

MRI of Pericardial Abnormalities

The pericardium is affected by various pathologic processes (Table 2) that result in variable clinical dysfunction.

Pericardial Effusion

Pericardial effusion is an accumulation of fluid in the pericardial sac beyond the normal physiologic amounts and results from a va-

TABLE 2: Various Pericardial Diseases

Imaging Finding	Differential Diagnosis
Fluid collection	Pericardial effusion, hematoma, cardiac tamponade
Inflammation	Pericarditis (acute inflammatory, chronic inflammatory, chronic fibrotic)
Pericardial constriction	Classic type or variant type[a]
Neoplasms	
Benign	Lipoma, teratoma, hemangioma, paraganglioma
Primary malignant	Sarcoma, mesothelioma, lymphoma
Secondary malignant	Metastases, lymphoma
Congenital	Pericardial cyst, congenital absence of pericardium
Miscellaneous	Pericardial diaphragmatic hernia

[a] Focal, normal thickness, effusive, inflammatory, occult, radiation.

riety of causes including cardiac or renal failure, infection, neoplasm, trauma, radiation, and myocardial infarction [12]. The accumulated fluid can be serous, fibrinous, purulent, or hemorrhagic. MRI is more sensitive than echocardiography in the detection of small collections, particularly those that are loculated (fibrinous, purulent, or hemorrhagic). In addition, MRI can assess the severity and location of the fluid collection, characterize the collection, assess its hemodynamic impact, detect associated inflammation or masses, and guide pericardiocentesis [2].

The earliest collection of pericardial fluid occurs adjacent to the posterolateral left ventricular wall or the inferolateral right ventricle wall, after which pericardial fluid accumulates in the superior recess [13]. Moderate-sized collections of fluid (100–500 mL) tend to accumulate in the anterior aspect of the right ventricle as well (> 5 mm) [2]. Large effusions are seen anterior to the right atrium and right ventricle, with an asymmetric ring of fluid around the heart. However, there is no direct correlation between the thickness of the pericardial cavity and the actual volume of the fluid because fluid does not spread homogeneously [2]. The volume of pericardial fluid can be quantified similar to quantification of ventricular volumes.

Simple, transudative effusions have low signal on T1-weighted images and high signal on T2-weighted FSE and SSFP images (Fig. 2). Complex effusions, such as exudative and hemorrhagic fluid, have high signal on T1-weighted and intermediate signal on T2-weighted spin-echo images. On SSFP images, fibrin strands or coagulated blood, often associated with loculations, can be seen. However, with the use of double–inversion recovery in FSE sequences, the signal depends on the presence of flow within the collection. Free-flowing collections such as transudates have no signal, but complex collections without flow have intermediate to high signal (Fig. 3). High signal can be seen on T1-weighted images even in simple effusion because of the nonlinear motion of fluid [2]. Complex effusions are seen in infections, hemopericardium, hypothyroidism, or malignancy. Hemopericardium may be seen secondary to rupture of the ascending aorta, acute aortic dissection, myocardial infarction, trauma, blood dyscrasia, anticoagulant therapy, and malignancy.

Occasionally, differentiating a small pericardial effusion from pericardial thickening may be difficult. However, careful analysis enables differentiation of these two MR findings (Table 3). Effusions have signal void on black blood sequences; show high signal on SSFP and gradient-echo images; have smooth margins; and follow a typical distribution pattern, which changes in configuration with decubitus positioning of the patient. In addition, an effusion loses myocardial tags with the cardiac cycle and does not have any contrast enhancement within it. Pericardial thickening is grayish to dark on T1-weighted, SSFP, and gradient-echo images; has irregular or nodular margins; and does not follow a typical distribution for effusion and shows no change with decubitus position of the patient. Myocardial tags persist throughout the cardiac cycle and may show contrast enhancement if inflamed [2].

Pericardial Hematoma

Pericardial hematoma is rare and typically follows cardiac surgery, pericardiocentesis, chest trauma, or epicardial injury [8]. At MRI, the signal depends on the age of the hematoma. In the subacute phase, a pericardial hematoma has heterogeneous high signal on T1- and T2-weighted sequences (Fig. 4) and low signal with a dark rim in the chronic phase. No contrast enhancement is seen [14]. Large hematomas can cause pericardial constriction, cardiac tamponade, or cardiac failure. The differential diagnosis includes pseudoaneurysm, neoplasm, and pericardial cyst.

Cardiac Tamponade

Cardiac tamponade is caused by acute accumulation of pericardial fluid (simple fluid, blood, pus), gas, or solid tissue, which results in an elevation of intrapericardial pressure, that decreases left ventricular filling and stroke volume. Common causes of cardiac tamponade are pericarditis, rupture after myocardial infarction, ruptured ventricular or coronary aneurysm or aortic aneurysm, dissection, thrombolytic therapy, large anterior mediastinal hematoma, blunt chest trauma,

TABLE 3: MRI Features That Differentiate Thickening and Effusion

Features	Effusion	Thickening
Signal in T1- and T2-weighted images	Signal void	Gray (except in calcification)
Signal in SSFP and GRE	High	Low
Margins	Smooth	Irregular or nodular
Location	Follows distribution typical of effusion	Does not follow typical distribution of effusion
Decubitus position	Change in configuration	No change in configuration
Tagging	Loss of tags with cardiac cycle	Persistent lines throughout cardiac cycle
Contrast enhancement	None	May be present if associated with inflamation

coronary artery bypass surgery, Dressler syndrome, endocarditis, and cardiac and paracardiac tumors [15].

The development of tamponade depends not only on the volume, but also on the rate of accumulation and the stiffness of the pericardium. Although a large effusion can accumulate without tamponade if it is a slow process, lesser amounts of fluid can cause tamponade if the accumulation is rapid. Chest discomfort and dyspnea are the common clinical symptoms. In the classic Beck triad, jugular venous distention, hypotension, and muffled heart sounds are present [1]. Tamponade is a clinical diagnosis that is suspected in patients with pulseless electrical activity or unexplained cardiogenic shock [1].

Although MRI is not used in the diagnosis of cardiac tamponade, cardiac tamponade may occasionally be encountered incidentally on MRI. MRI shows the fluid, gas, or tumor in the pericardial space. In addition, the SVC, inferior vena cava (IVC), and hepatic veins are dilated. The anterior surface of the heart is flat with diminished anteroposterior diameter (i.e., "flattened heart" sign). In severe cases, there is diastolic inversion—that is, collapse of the right ventricle free wall in early diastole and collapse of the right atrium free wall during late diastole and early systole (Figs. 5A and S5B [Fig. S5B, a cine loop, can be viewed from the online version of this article at www.ajronline.org.]). Diastolic inversion occurs in early diastole because there is more blood in the right atrium than right ventricle and the lower pressure in the right ventricle makes it vulnerable against the high pressure of effusion. In late diastole and systole, there is less blood in the right atrium, making it vulnerable against the high-pressure pericardial fluid collection. Because right heart filling is reduced during expiration, right-sided collapse is prominent during this respiratory phase [1, 15]. In severe cases, the cardiac chambers are compressed, along with compression of the coronary sinus, pulmonary trunk, or IVC. Septal rocking, sigmoid interventricular septum (convexity to the left ventricle), and exaggerated respiratory variation in cardiac inflow and outflow patterns in the SVC and IVC are other signs of cardiac tamponade [15].

Pericarditis

Pericarditis is inflammation of the pericardium that can be idiopathic (30%) or caused by various abnormalities, such as infections (viral, bacterial, fungal, tuberculosis); connective tissue diseases (systemic lupus erythematosus, rheumatoid arthritis, systemic sclerosis); radiation; uremia; myocardial infarction (early [epistenocardiac] or Dressler syndrome). The clinical symptoms depend on the severity of inflammation. MRI is not required when the clinical findings are classic, but it is required in atypical presentations, particularly when there is failure of response to therapy; a complicated course, such as chronic or recurrent pericarditis with or without constriction; a traumatic cause; or other specific disease processes. MRI is also used to monitor the response to antiinflammatory therapy, particularly in patients with recurrence or constriction, to balance the risk of recurrence with the risk of side effects of drug therapy. Even if clinical and serologic tests are negative, the presence of pericardial inflammation on MRI warrants continued therapy [1].

Acute pericarditis—Acute pericarditis is characterized pathologically by the presence of vascularized granulation tissue, fibrin, and fluid. Clinically, it presents with pleuritic-type retrosternal chest pain that is worse with inspiration and in supine position and is often associated with a friction rub on auscultation [1]. MRI shows pericardial thickening and effusion. Thickening has grayish signal and effusion has low signal on T2-weighted FSE sequences. On SSFP images, intermediate signal is seen because of pericardial thickening and high signal is seen because of simple pericardial effusion. STIR images show high signal of pericardial fluid or pericardial edema. Immediate and delayed contrast-enhanced images show contrast enhancement due to inflammation (Fig. 6), which may extend to adjacent epicardial fat or myocardium [16, 17]. This inflammation may be diffuse or focal (Fig. 7).

Multiple images in various planes are essential for a comprehensive evaluation of the entire pericardium, particularly in the evaluation of focal pericarditis. Occasionally there is no significant pericardial thickening, but there is contrast enhancement of the pericardium or the epicardial fat (Fig. 8).

Chronic inflammatory pericarditis—Chronic inflammatory pericarditis is characterized by accumulation of fibroblasts and of collagen and by less fibrin deposition. MRI shows irregularly thickened pericardium with mild effusion. Variable contrast enhancement is seen (Fig. 9). Occasionally exuberant epicardial fat is seen, which might be a chronic inflammatory response (Fig. 10).

Chronic fibrosing pericarditis—Chronic fibrosing pericarditis is characterized by the presence of fibroblasts and collagen, which eventually result in calcific and noncompliant pericardium. MRI shows thick pericardium, which has low signal on all the sequences because of fibrosis or calcification. Pericardial fluid is either minimal or absent. Contrast enhancement is absent except in a few cases with residual inflammation. Features of pericardial constriction, which are discussed in the next section, may be present.

Pericardial Constriction

Pericardial constriction is caused by thickened, fibrotic or calcified, nonelastic pericardium that impairs left ventricle diastolic filling and results in elevated systemic venous pressures and low cardiac output. It is a sequela of the various causes of pericarditis discussed in the previous section. Constriction can develop acutely, but more often it is a slow process (3–12 months) [1]. Although it typically affects the parietal pericardium, pericardial constriction can occasionally involve only the visceral layer [11]. Clinical features are caused by low cardiac output (fatigue, hypotension, and tachycardia), elevated systemic venous pressure (jugular venous distention, hepatomegaly, ascites, and edema), and pulmonary venous congestion (dyspnea, orthopnea, and cough). The Kussmaul sign and diastolic pericardial knock are present.

The diagnosis of pericardial constriction can be challenging and it often requires the use of multiple imaging modalities, of which MRI plays a significant role. MRI can differentiate constriction from the clinically similar restrictive cardiomyopathy. In addition, MRI can exclude other causes of right heart failure, such as pulmonary hypertension, shunts, right ventricle dysplasias, and right ventricle infarction; determine if thickened, inflamed, or nonthickened pericardium is causing constriction; and evaluate whether the patient will benefit from pericardial stripping [2].

Pericardial thickening (> 4 mm) is an indicator of constriction in patients with the appropriate symptoms and signs of right heart failure. Pericardial thickening is more pronounced on the right side, particularly surrounding the right ventricle and the anterior atrioventricular groove [2]. However, thickening does not always imply constriction. Thickening can be seen after acute pericarditis or cardiac surgeries without physiologic changes of constriction [12]. Occasionally constriction can be seen without thickening. Con-

trast enhancement indicates the presence of inflammation. Constriction is more common on the right side because thickening is more common on the right side and the right ventricle has a thin wall. Long-standing constriction results in conical deformity of the ventricles (Fig. 11A). Other findings of constriction due to elevated cardiac filling pressures are seen: biatrial enlargement (Fig. 11B); narrow atrioventricular groove; dilated SVC, IVC, and hepatic veins; pleural effusion; and ascites. In the SVC, systolic flow is decreased, absent, or reversed, but in diastole, forward flow is increased with increased late backflow (Fig. 11C).

In patients with constriction, pericardial motion is reduced or is even absent during the cardiac cycle, unlike healthy persons where the pericardium moves synchronous with the cardiac cycle. There is tethering and restricted ventricular expansion adjacent to thickened areas. These findings can also be shown using tagging. Tag lines are typically displaced during the cardiac cycle in healthy persons because of the free motion of the pericardium, whereas in patients with pericardial constriction, the tag lines are stretched and fail to break because of restricted motion between the pericardial layers. Systolic myocardial contraction is usually normal [18, 19]. The following functional abnormalities due to rigid fixed pericardial volume are seen in patients with pericardial constriction: dissociation between intrathoracic and intracardiac pressures, increased filling pressures with equalization of end-diastolic pressures in all chambers, increased ventricular coupling influenced by respiration, elevated systemic venous pressures, and low cardiac output. Although ventricular filling is determined by compliance of cardiac chambers in healthy persons, in patients with pericardial constriction, ventricular filling is limited by pericardial volume; once the constraining volume is reached, there is abrupt cessation of diastolic filling. Ventricular filling can be detected visually on a four-chamber (Fig. S11D [a cine loop]) or short-axis cine image or can be quantified by plotting ventricular volumes against time or by using velocity-encoded phase-contrast MRI in the form of increased early filling and decreased or absent late filling.

Diastolic interventricular septal flattening is a finding that has a sensitivity of 62–81% and specificity of 93–100% for constriction [20] in the diagnosis of constriction. In healthy persons, the ventricular septum is not flat: It is convex to the right side because of higher left ventricular pressure, resulting in a positive left-to-right transseptal pressure gradient throughout the cardiac cycle with only minimal respiratory variation. In patients with pericardial constriction, outward expansion of the right ventricle during the early right ventricle filling (which precedes left ventricle filling) is limited by a noncompliant rigid pericardium, resulting in increased right ventricle pressure; when transmitted to the compliant septum, this increased pressure produces septal flattening or even transient inversion to the left side ("diastolic septal bounce") in early diastolic filing. However, rarely minimal septal flattening may be seen in healthy persons. Diastolic bounce is also seen in conditions of right ventricle volume overload and cor pulmonale and in patients after cardiac surgeries due to bundle-branch blocks.

Respiratory variation in this septal movement is a pathognomonic feature of pericardial constriction. In healthy persons, inspiration reduces the intrathoracic pressure that is transmitted to the cardiac chambers, resulting in a constant driving pressure from the lungs across the pulmonary veins into the left atrium and across the mitral valve. However, in patients with pericardial constriction, the rigid pericardium results in dissociation between intrathoracic and intracardiac pressures; the negative intrathoracic pressure is not transmitted to the left heart chambers, so there is less driving force from the lungs into the left ventricle. Hence, with inspiration, the negative intrathoracic pressure increases venous return turn more on the right side but because of right ventricle outward motion and filling, is impaired, resulting in septal flattening and paradoxical motion of septum to left [21]. With expiration, there is positive intrathoracic pressure that reduces systemic but increases pulmonary return, which will result in septal bowing to the right side [22]. This finding can be detected on MRI using a real-time imaging sequence in the short-axis plane (Fig. S11E [a cine loop]) and has 81% sensitivity, 100% specificity, 90% accuracy, 100% positive predictive value, and 83% negative predictive value in the diagnosis of pericardial constriction [23, 24]. A septal excursion of 11.8% was very useful in differentiating constriction from restriction [24]. It is best seen in the base and in the first heartbeat after inspiration. This finding is not seen in restrictive cardiomyopathy or cor pulmonale. It may be absent in focal constriction [24].

Variants of Pericardial Constriction

Focal pericardial constriction—Strategically located focal thickening, such as in the atrioventricular groove and basal ventricles, can also produce features of pericardial constriction which may be subtle on MRI (Figs. 12A and S12B [Fig. S12B, a cine loop, can be viewed from the online version of this article at www.ajronline.org.]). A comprehensive evaluation of the pericardium should include perpendicular views through the entire pericardium in multiple planes [2].

Constriction with normal-thickness pericardium—In 18% of patients with pericardial constriction, constriction is seen with a normal-thickness but noncompliant pericardium. These patients will also benefit from pericardectomy [25] (Fig. 13).

Effusive constrictive pericarditis—Effusive constrictive pericarditis is a rare syndrome in which there is tamponade caused by tense effusion and constriction caused by inflamed and noncompliant visceral pericardium [1]. It can be idiopathic or seen in malignancies and after radiation. Features of constriction persist even after removal or resolution of pericardial fluid. It is possibly an intermediate phase in the transition from acute pericarditis with effusion to pericardial constriction. Patients with effusive constrictive pericarditis may have improvement of symptoms, either spontaneously or after treatment with antiinflammatory drugs [26].

Inflammatory constrictive form—Constriction is occasionally seen during the resolution phase of acute idiopathic pericarditis because of a noncompliant pericardium. There are no signs of clinical activity with minimal residual or no pericardial effusion. This form of constriction is usually transient, subsides in a few months, and is possibly an intermediate stage between spontaneous resolution and evolution to constriction [2].

Occult constrictive pericarditis—Occasionally constriction is not obvious during routine examination but manifests when there is a rapid fluid challenge [2].

Radiation pericarditis—Pericardial constriction and restrictive cardiomyopathy may coexist in patients with radiation heart disease, which makes the diagnosis challenging. The presence of systolic failure in these patients is a marker of poor prognosis after pericardectomy.

Table 4 summarizes the salient characteristics of various types of pericarditis.

TABLE 4: Features of Various Types of Pericarditis

Type	Pathology	Thickening	Effusion	Enhancement	Ventricular Coupling
Acute pericarditis	Vascularized granulation tissue, fibrin, fluid	Present	May be seen	Pericardial layers enhance; epicardial fat and myocardium may enhance	Absent
Chronic inflammatory pericarditis	Fibroblasts, collagen, less fibrin	Present	May be mild	Pericardial layers enhance; epicardial fat and myocardium may enhance	Absent
Chronic fibrosing pericarditis	Fibroblasts, collagen, calcification, stiff with constriction	Present; dark if fibrosed or calcified	Absent	Absent	May be present if associated with constriction
Effusive constrictive pericarditis	Effusion, inflamed pericardium, noncompliant visceral pericardium	May be thickened	Moderate-to-large effusion	May be mild enhancement	Present
Inflammatory constrictive pericarditis	Constriction during acute and chronic inflammation, noncompliant pericardium; may be transient	Present	May be mild	Pericardial layers enhance; epicardial fat and myocardium may enhance	Present; transient
Focal pericarditis	Focal areas of inflammation or fibrosis; may produce constriction if in strategic location	Focal	May be seen	Focal enhancement may be seen	May be present if in strategic location

Pericardial Neoplasms

Pericardial neoplasms are uncommon, with secondary neoplasms more common than primary neoplasms. MRI is useful in the diagnosis, characterization, and delineation of the extent of disease and spread of disease to adjacent structures. The following findings indicate aggressive disease: disrupted pericardium; hemorrhagic effusion; invasion into epicardial fat, myocardium, or cardiac chambers; and associated mediastinal or pericardial lymphadenopathy [1]. Hematoma and gossypiboma produce a mass-like appearance.

Pericardial metastasis—Pericardium is more often involved by metastatic disease than primary pericardial neoplasms [2]. Pericardial metastasis occurs in 10% of patients with malignancies, particularly in those with cancers of the lung, breast, esophagus, and kidney and those with melanoma, leukemia, multiple myeloma, lymphoma, and thymoma. Spread to the pericardium can occur hematogenously or through lymphatics or by direct invasion from adjacent structures. At MRI, pericardial metastasis is seen as a large hemorrhagic pericardial effusion, irregular or nodular pericardial thickening (Fig. 14A), nodules, or masses (Fig. 14B). A malignant effusion is often large and complex. Except melanoma metastases, which have high signal on T1-weighted images, nodules and masses have intermediate signal on T1-weighted images and high signal on T2-weighted images. Contrast enhancement is variable and heterogeneous. Spread into adjacent structures can be noted. Cardiac failure is seen in one fourth of patients, and death is usually secondary to cardiac tamponade [27, 28].

Primary benign pericardial neoplasms—Benign pericardial neoplasms include lipoma, teratoma, fibroma, hemangioma, lymphangioma, neurofibroma, paraganglioma, and granular cell myoblastoma.

Lipoma is a neoplasm of mature adult fat cells that commonly occurs in middle-aged and older adults. It originates either from the subendocardial layer of the heart or from the subepicardial or myocardial layer and extends into the pericardium. At MRI, lipoma has homogeneous signal intensity similar to fat on all the sequences—that is, high on T1-weighted, intermediate on T2-weighted, and signal dropout on fat-suppressed sequences [27]. Large tumors can cause cavitary obstruction, compressive effects, and arrhythmias. Teratoma has cystic or solid components with areas of fat and calcification.

Hemangioma is characterized by proliferation of vascular spaces that are lined by an endothelial layer. At MRI, hemangioma is seen as a heterogeneous mass, with intermediate-to-high signal on T1-weighted images because of slow flow and high signal intensity on T2-weighted images (Fig. 15). Contrast enhancement is heterogeneous and intense except in low-flow lesions [29].

Paraganglioma is a functioning chromaffin cell tumor originating from parasympathetic ganglia in the roof of the left atrium or in the interatrial septum. It is more common in young adults in the third and fourth decades. At MRI, flow voids are seen on T1-weighted spin-echo images because of intense vascularity. High signal on T2-weighted images and marked contrast enhancement are also seen [28, 29] (Fig. 16).

Primary pericardial malignant neoplasms—Malignant pericardial neoplasms include mesothelioma, sarcoma, lymphoma, malignant teratoma, and hemangioendothelioma.

Mesothelioma accounts for 50% of primary pericardial malignancies and is believed to arise secondary to asbestos exposure. At MRI, it is seen as nodules, masses, diffuse plaque, or hemorrhagic pericardial effusion. Pericardium may be also be involved secondarily by a pleural mesothelioma. Sarcoma is occasionally seen in the pericardium and could be angiosarcoma, fibrosarcoma, malignant fibrous histiocytoma, or liposarcoma. At MRI, sarcoma can be seen as an irregular, nodular, broad-based mass with heterogeneous enhancement and pericardial thickening or complex effusion. Primary cardiac lymphoma is less common than secondary cardiac involvement, accounting for 1.3% of cardiac neoplasms. It is usually of the high-grade B-cell type and is secondary to immunodeficiency such as in HIV infection. The commonly affected sites include the right atrium, pericardium, subepicardial fat, and atrioventricular groove. At MRI, pericardial effusion, nodules, or masses can be seen with heterogeneous enhancement. Mediastinal lymphadenopathy may also be present [29].

Pericardial Cyst

A pericardial cyst is a developmental abnormality that is caused by pinching-off of a blindly ending parietal pericardial recess. Pericardial cyst is asymptomatic, but it can occasionally produce chest pain or dyspnea when it compresses the heart. The right cardiophrenic angle is the most common loca-

tion for a pericardial cyst (80% of cases), although it can occasionally be seen in the left cardiophrenic angle or in the mediastinum. At MRI, a pericardial cyst is seen as a well-defined and sharply marginated, homogeneous unilocular cyst with low signal on T1-weighted images and high signal on T2-weighted images (Fig. 17A) with no contrast enhancement. High signal may be seen on T1-weighted images if the content is proteinaceous, and very rarely a lobulated margin is seen (Fig. 17B).

A pericardial diverticulum has an origin similar to that of a pericardial cyst, but unlike a cyst, a pericardial diverticulum communicates with the pericardial cavity; as a result, the wall is incomplete on the medial aspect.

Other common lesions that mimic a pericardial cyst include enlarged lymph nodes, loculated fluid collection, hematoma, and necrotic tumor. Less common causes include bronchogenic cyst, cystic teratoma, cystic neurogenic tumor, cystic lymphangioma, thoracic duct cyst, and thymic cyst [2, 8].

Congenital Absence of Pericardium

Congenital absence of pericardium is a rare (0.002–0.004%) [2, 30] developmental abnormality that is caused by premature atrophy of the left common cardinal vein, resulting in loss of blood supply to the left pleuropericardial membrane that forms the left pericardium. Because the right common cardinal vein typically persists as the SVC, the right side of the pericardium is assured of good blood supply, thus sparing the right side [31]. Congenital absence is typically partial, but occasionally it is complete. It is more common in the left (70%) than the right (17%) or inferior aspects [8]. It is usually asymptomatic, but symptoms are seen when complications develop. It is associated with other malformations such as atrial septal defect; tetralogy of Fallot; patent ductus arteriosus; mitral stenosis; and malformations of the lung, chest wall, and diaphragm [8].

At MRI, there is absence of the entire pericardium or a portion of it. However, either finding alone is not sufficient to make a diagnosis of congenital absence because pericardium over the left atrial appendage and left ventricle is not clearly identified even in healthy individuals because of the paucity of fat and low signal intensity from adjacent lungs. A diagnosis of congenital absence should not be made without mediastinal shift or regional bulging. The heart is displaced to the left and posterior aspects (levorotation). Levorotation can also be seen in other conditions such as pulmonary stenosis, mitral valve disease, and cor pulmonale and occasionally can be seen in cases of partial absence. Pericardium might be absent in young children with a complete defect.

Interposition of lung tissue between the aorta and pulmonary artery or between the diaphragm and base of the heart is a characteristic finding of congenital absence. The pulmonary artery may be enlarged with a change in the axis of the main pulmonary artery and left atrial appendage. A normal cardiac apex is relatively stationary with the cardiac cycle, but in congenital absence, there is excessive myocardial mobility (15 mm instead of the normal 1.7 mm); excessive myocardial mobility can also be observed on images acquired with the patient in left and right lateral decubitus positions. In addition, the difference between end-systolic and end-diastolic volumes (normal difference, 5–11%) is exaggerated [30].

The heart and lung can herniate through the defect. Herniation of the left atrial appendage may result in strangulation, whereas herniation of the left coronary artery may result in myocardial ischemia or infarction. The risk of traumatic aortic dissection is increased because of cardiac displacement and mobility. Surgical pericardioplasty is required in patients with large herniations and in those with imminent strangulation [30].

Pericardial Diaphragmatic Hernia

Intrapericardial diaphragmatic hernia is a rare condition in which the stomach, bowel, or abdominal fat herniates into the pericardial sac. This condition could be congenital, traumatic, or iatrogenic. Blunt or penetrating trauma is the most common cause (Fig. 18). Congenital defects are caused by failure of the septum transversum. Iatrogenic defects may be seen after coronary bypass surgery and pericardial window or pacemaker insertion through an abdominal approach. The clinical presentation is variable. Complications include cardiac tamponade, bowel strangulation, and ischemia [32].

Conclusion

MRI is a vital diagnostic tool in the evaluation of pericardial diseases, particularly inflammation and constriction, providing both morphologic and functional information (Table 3) essential for determining the optimal therapeutic strategy. It is used for the characterization and delineation of the extent of spread of pericardial masses. Various imaging sequences are available, which should be optimized and tailored to the specific clinical condition that is being evaluated.

References

1. Verhaert D, Gabriel RS, Johnston D, Lytle BW, Desai MY, Klein AL. The role of multimodality imaging in the management of pericardial disease. *Circ Cardiovasc Imaging* 2010; 3:333–343
2. Bogaert J, Francone M. Cardiovascular magnetic resonance in pericardial diseases. *J Cardiovasc Magn Reson* 2009; 11:14
3. Lewis WH. The pericardium. In: Gray H, ed. *Anatomy of the human body.* Philadelphia, PA: Lea & Febiger, 1918
4. Roberts WC, Spray TL. Pericardial heart disease: a study of its causes, consequences, and morphologic features. *Cardiovasc Clin* 1976; 7:11–65
5. Broderick LS, Brooks GN, Kuhlman JE. Anatomic pitfalls of the heart and pericardium. *RadioGraphics* 2005; 25:441–453
6. Olson MC, Posniak HV, McDonald V, et al. Computed tomography and magnetic resonance imaging of the pericardium. *RadioGraphics* 1989; 9: 633–649
7. Lopez Costa I, Bhalla S. Computed tomography and magnetic resonance imaging of the pericardium. *Semin Roentgenol* 2008; 43:234–245
8. Rajiah P, Kanne JP. Computed tomography of the pericardium and pericardial disease. *J Cardiovasc Comput Tomogr* 2010; 4:3–18
9. Rienmuller R, Groll R, Lipton MJ. CT and MR imaging of pericardial disease. *Radiol Clin North Am* 2004; 42:587–601
10. Al-Mallah M, Kwong RY. Assessing pericardial disease with CMR. In: Kwong RY, ed. *Cardiovascular magnetic resonance imaging.* Totowa, NJ: Humana Press, 2007:467–490
11. Spodick DH. Pericardial macro- and microanatomy: a synopsis. In: Spodick DH, ed. *The pericardium: a comprehensive textbook.* New York, NY: Marcel Dekker, 1997:7–14
12. Wang ZJ, Reddy GP, Gotway MB, Yeh BM, Hetts SW, Higgins CW. CT and MR imaging of pericardial disease. *RadioGraphics* 2003; 23(spec no):S167–S180
13. Stark DD, Higgins CB, Lanzer P, et al. Magnetic resonance imaging of the pericardium: normal and pathologic findings. *Radiology* 1984; 150: 469–474
14. Smith WH, Beacock DJ, Goddard AJ, Bloomer TN, Ridgeway JP, Sivanathan UM. Magnetic resonance evaluation of the pericardium. *Br J Radiol* 2001; 74:384–392
15. Restrepo CS, Lemos DF, Lemos JA, et al. Imaging findings in cardiac tamponade with emphasis on CT. *RadioGraphics* 2007; 27:1595–1610
16. Yelgec NS. Dymarkowski S, Ganame J, et al. Value of MRI in patients with a clinical suspicion of acute myocarditis. *Eur Radiol* 2007; 17:2211–2217

17. Taylor AM, Dymarkowski S, Verbeken E, Bogaert J. Detection of pericardial inflammation with late enhancement cardiac magnetic resonance imaging: initial results. *Eur Radiol* 2006; 16:569–574
18. Napolitano G, Pressacco J, Paquet E. Imaging features of constrictive pericarditis: beyond pericardial thickening. *Can Assoc Radiol J* 2009; 60:40–46
19. Kojima S, Yamada N, Goto Y. Diagnosis of constrictive pericarditis by tagged cine magnetic resonance imaging. *N Engl J Med* 1999; 341:373–374
20. Ghersin E, Lessick J, Litmanovich D, et al. Septal bounce in constrictive pericarditis: diagnosis and dynamic evaluation with multidetector CT. *J Comput Assist Tomogr* 2004; 28:676–678
21. Hurrell DG, Nishimura RA, Higano ST, et al. Value of dynamic respiratory changes in left and right ventricular pressures for diagnosis of constrictive pericarditis. *Circulation* 1996; 93:2007–2013
22. Ariyarajah V, Jassal DS, Kirkpatrick I, Kwong RY. The utility of cardiovascular magnetic resonance in constrictive pericardial disease. *Cardiol Rev* 2009; 17:77–82
23. Francone M, Dymarkowski S, Kalantzi M, Rademarkers FE, Bogaert J. Real-time cine MRI of ventricular septal motion: a novel approach to assess ventricular coupling. *J Magn Reson Imaging* 2005; 21:305–309
24. Francone M, Dymarkowski S, Kalantzi M, Rademarkers FE, Bogaert J. Assessment of ventricular coupling with real-time cine MRI and its value to differentiate constrictive pericarditis from restrictive cardiomyopathy. *Eur Radiol* 2006; 16:944–951
25. Talreja DR, Nishimura RA, Oh JK, Holmes DR. Constrictive pericarditis in the modern era: novel criteria for diagnosis in the cardiac catheterization laboratory. *J Am Coll Cardiol* 2008; 51:315–319
26. Sagristà-Sauleda J, Angel J, Sánchez A, Permanyer-Miralda G, Soler-Soler J. Effusive-constrictive pericarditis. *N Engl J Med* 2004; 350:469–475
27. Grizzard JD, Ang GB. Magnetic resonance imaging of pericardial disease and cardiac masses. *Magn Reson Imaging Clin N Am* 2007; 15:579–607, vi
28. Grebenc ML, Rosado de Christenson ML, Burke AP, Green CE, Galvin JR. Primary cardiac and pericardial neoplasms: radiologic-pathologic correlation. *RadioGraphics* 2000; 20:1073–1103
29. Sparrow PJ, Kurian JB, Jones TR, Sivananthan MU. MR imaging of cardiac tumors. *RadioGraphics* 2005; 25:1255–1276
30. Psychidis-Papakyritisis P, de Roos A, Kroft LJM. Functional MRI of congenital absence of the pericardium. *AJR* 2007; 189:1370; [web]W312–W314
31. Von Son JA, Danielson GK, Schaff HV, Mullany CJ, Julsrud PR, Breen JF. Congenital partial and complete absence of the pericardium. *Mayo Clin Proc* 1993; 68:743–747
32. Drafts BC, Chughtai HL, Entrikin DW. Iatrogenic intrapericardial diaphragmatic hernia diagnosed by cardiovascular magnetic resonance. *J Cardiovasc Magn Reson* 2010; 12:3

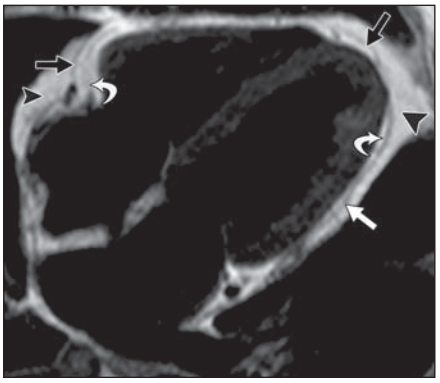

Fig. 1—Appearance of normal pericardium on black blood imaging. Four-chamber T2-weighted double–inversion recovery black blood fast spin-echo image of 34-year-old woman shows intermediate-signal band of pericardium (*straight arrows*) situated between high signal of epicardial fat (*curved arrows*) and mediastinal fat (*arrowheads*).

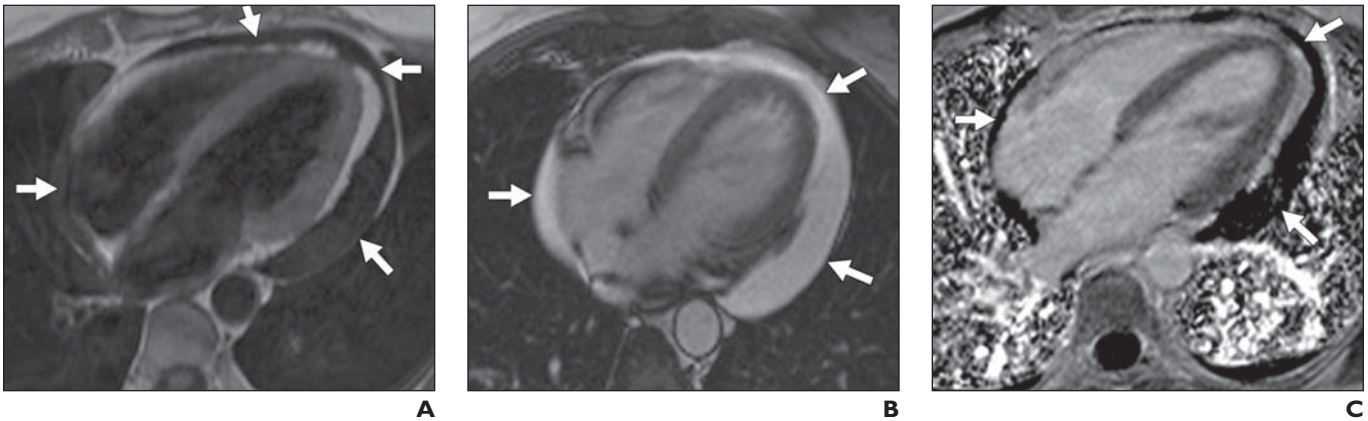

Fig. 2—Pericardial effusion in 28-year-old man.
A, Four-chamber T2-weighted double–inversion recovery black blood image shows moderate circumferential pericardial effusion (*arrows*) with low signal intensity, most over posterolateral aspect of left ventricle.
B, Four-chamber steady-state free precession image shows moderate pericardial effusion (*arrows*) with high signal intensity over lateral aspect of left ventricle.
C, Phase-sensitive inversion recovery delayed enhancement image shows effusion (*arrows*) as dark collection.

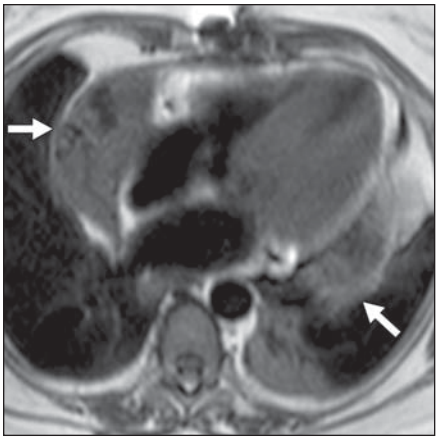

Fig. 3—Complex pericardial effusion. Axial T2-weighted double–inversion recovery image of 63-year-old woman who presented with chest pain and dyspnea after aortic valve replacement shows two loculated fluid collections (*arrows*) having heterogeneously low signal intensity adjacent to right atrium and left ventricle.

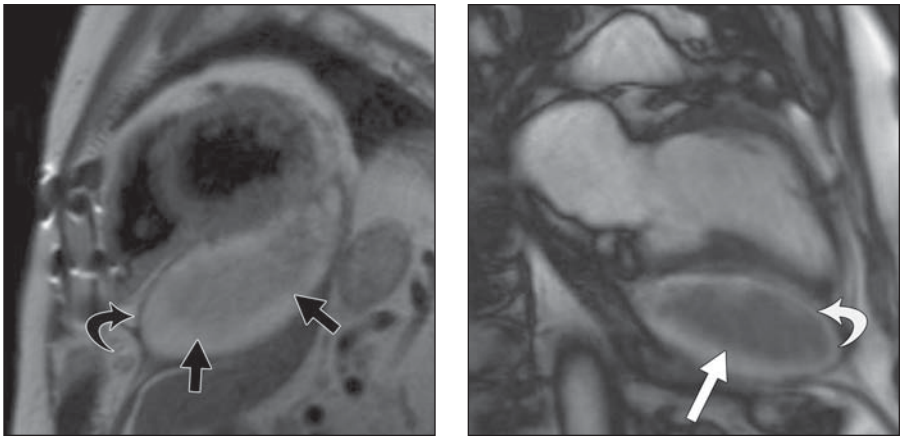

Fig. 4—Hemopericardium in 83-year-old man with history of recent myocardial infarction.
A, Short-axis T2-weighted black blood image shows heterogeneous fluid collection with intermediate to high signal (*straight arrows*) between thickened layers of pericardium (*curved arrow*).
B, Two-chamber steady-state free precession image shows heterogeneous hematoma (*straight arrow*) between pericardial layers (*curved arrow*) caused by rupture of heart.

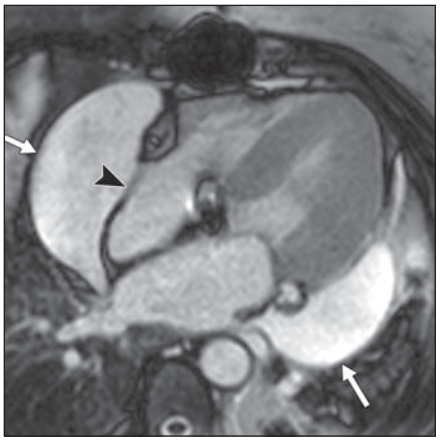

Fig. 5—Focal cardiac tamponade. Figure S5B, cine loop, can be viewed from online version of this article available at www.ajronline.org. Four-chamber steady-state free precession image of 63-year-old woman obtained after aortic valve replacement shows two loculated effusions (*arrows*) having high signal intensity adjacent to right atrium and left ventricle. In addition, there is collapse of right atrial wall during diastole (*arrowhead*), which is indicative of focal cardiac tamponade.

Fig. 6—Diffuse acute pericarditis in 42-year-old woman with systemic lupus erythematosus. Short-axis phase-sensitive inversion recovery image shows diffuse enhancement of thickened parietal (*straight white arrows*) and visceral (*straight black arrows*) pericardium enclosing dark pericardial effusion (*curved arrow*); these findings are consistent with acute pericarditis.

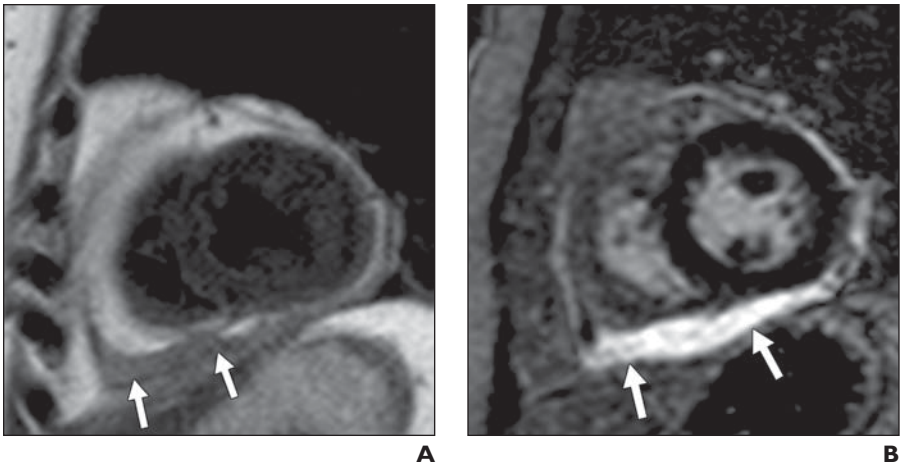

Fig. 7—Focal acute pericarditis in 60-year-old woman with chest pain.
A, Short-axis T2-weighted double–inversion recovery black blood image shows focal pericardial thickening (*arrows*) in inferior aspect of left ventricle.
B, Short-axis phase-sensitive inversion recovery image shows marked enhancement of pericardium adjacent to inferior wall (*arrows*); these findings are consistent with focal acute pericarditis.

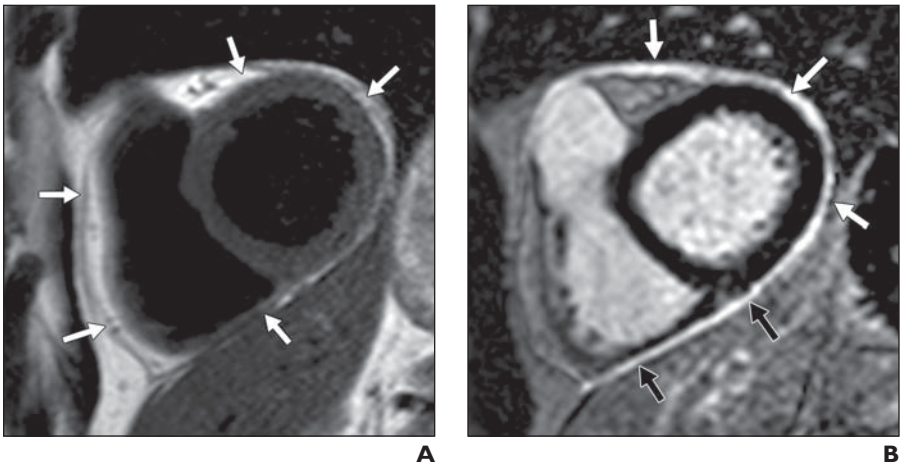

Fig. 8—Pericardial enhancement without thickening in 39-year-old man presenting with chest pain.
A, Short-axis T2-weighted double–inversion recovery black blood image shows pericardium with normal thickness (*arrows*).
B, Short-axis phase-sensitive inversion recovery image shows diffuse circumferential high signal of pericardium (*arrows*) and of epicardial fat layers; these findings are suggestive of inflammation.

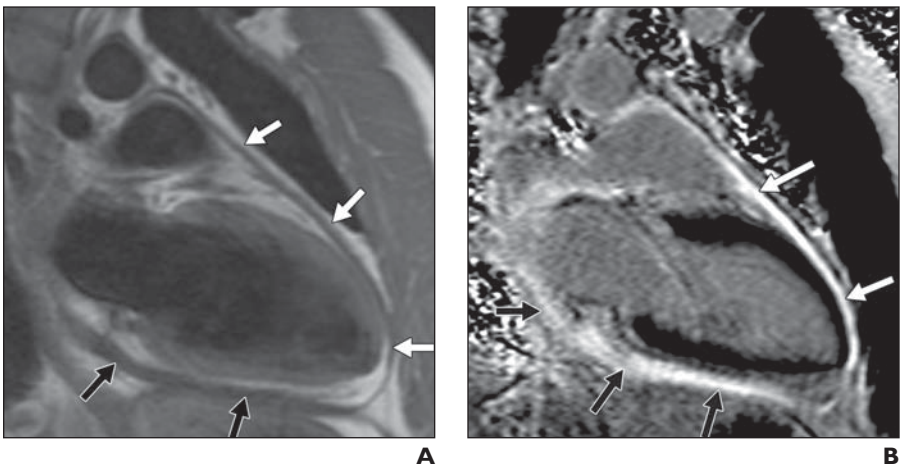

Fig. 9—Chronic inflammatory pericarditis in 45-year-old man with chest pain.
A, Vertical long-axis T2-weighted double–inversion recovery black blood image shows diffuse circumferential pericardial thickening (*arrows*) without any effusion.
B, Vertical long-axis phase-sensitive inversion recovery image shows marked diffuse circumferential enhancement of pericardium (*arrows*) consistent with chronic inflammation.

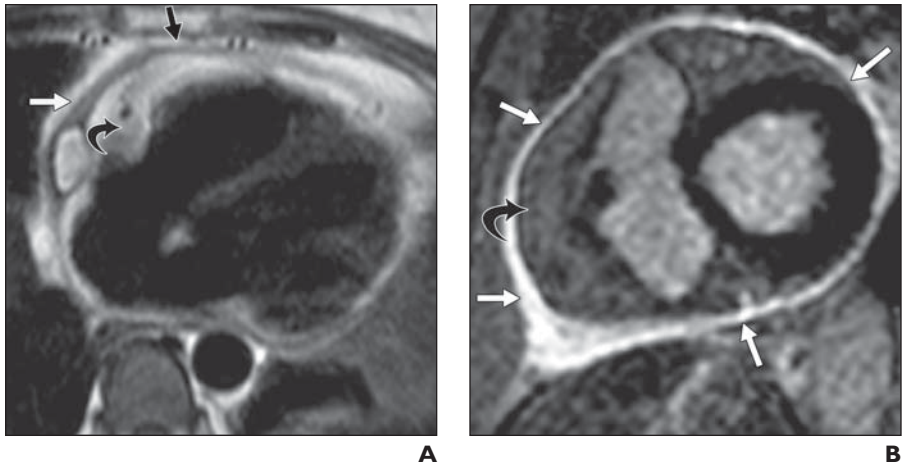

Fig. 10—Pericarditis with prominent fat in 57-year-old woman with history of breast cancer who presented with chest pain.
A, Four-chamber T2-weighted black blood double–inversion recovery image shows circumferential pericardial thickening (*straight arrows*). In addition, there is exuberant pericardial fat (*curved arrow*).
B, Short-axis phase-sensitive inversion recovery image shows diffuse circumferential pericardial enhancement (*straight arrows*). In addition, there is exuberant epicardial fat (*curved arrow*) probably due to inflammatory response.

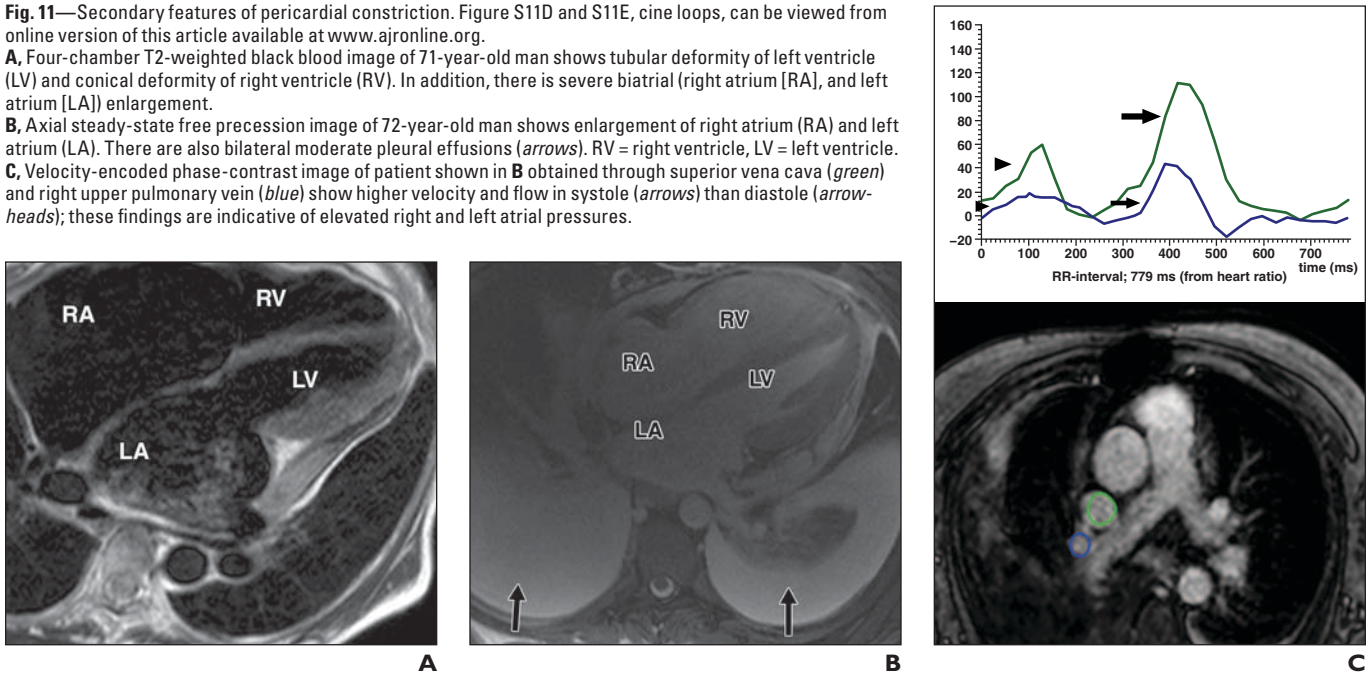

Fig. 11—Secondary features of pericardial constriction. Figure S11D and S11E, cine loops, can be viewed from online version of this article available at www.ajronline.org.
A, Four-chamber T2-weighted black blood image of 71-year-old man shows tubular deformity of left ventricle (LV) and conical deformity of right ventricle (RV). In addition, there is severe biatrial (right atrium [RA], and left atrium [LA]) enlargement.
B, Axial steady-state free precession image of 72-year-old man shows enlargement of right atrium (RA) and left atrium (LA). There are also bilateral moderate pleural effusions (*arrows*). RV = right ventricle, LV = left ventricle.
C, Velocity-encoded phase-contrast image of patient shown in **B** obtained through superior vena cava (*green*) and right upper pulmonary vein (*blue*) show higher velocity and flow in systole (*arrows*) than diastole (*arrowheads*); these findings are indicative of elevated right and left atrial pressures.

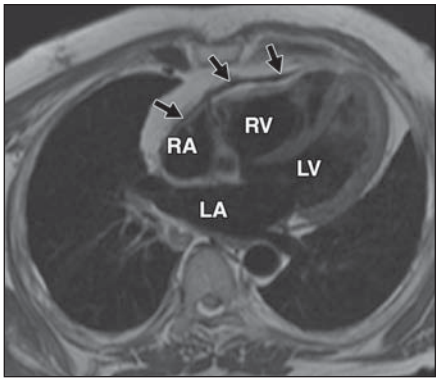

Fig. 12—Focal constriction in 49-year-old man. Figure S12B, cine loop, can be viewed from online version of this article available at www.ajronline.org. Four-chamber T2-weighted double–inversion recovery prepared black blood image shows focal thickening of pericardium (*arrows*) overlying right atrium (RA) and right ventricle (RV). Note the tubular deformity of ventricles. Cine images showed diastolic restraint and inspiratory septal flattening. LA = left atrium, LV = left ventricle.

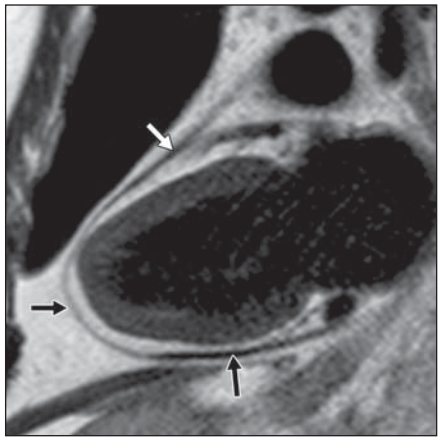

Fig. 13—Constriction without thickening in 37-year-old patient with chest pain and generalized body wall edema. Two-chamber T2-weighted double–inversion recovery black blood image shows normal-thickness pericardium (*arrows*). Diastolic restraint and inspiratory septal flattening were seen in cine images.

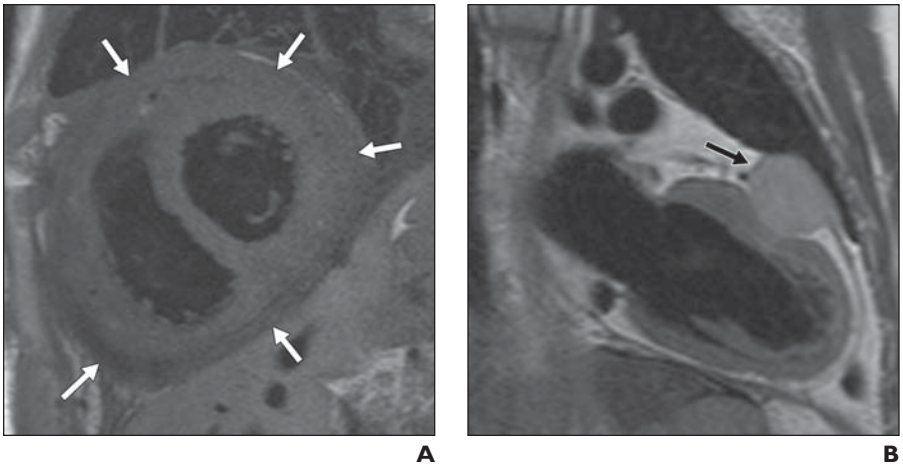

Fig. 14—Pericardial metastasis.
A, Short-axis T2 black blood image of 57-year-old woman with history of breast cancer shows diffuse circumferential intermediate-signal-intensity mass (*arrows*) is encasing ventricles.
B, Two-chamber T2-weighted black blood image of 64-year-old man with history of synovial sarcoma shows homogeneous intermediate-signal-intensity metastatic mass (*arrow*) in pericardium. Mass is indenting underlying anterior wall of left ventricle. Note mild pericardial thickening.

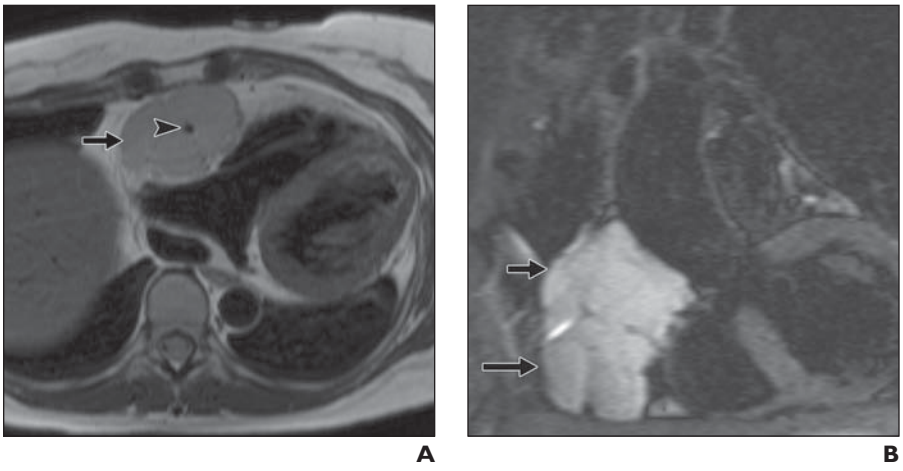

Fig. 15—Pericardial hemangioma in 46-year-old woman.
A, Axial four-chamber T2-weighted black blood image shows homogeneous intermediate-signal-intensity mass in right atrioventricular groove (*arrow*) encasing right coronary artery (*arrowhead*).
B, Coronal T2 STIR image shows lobulated high-signal-intensity mass in right atrioventricular groove (*arrows*).

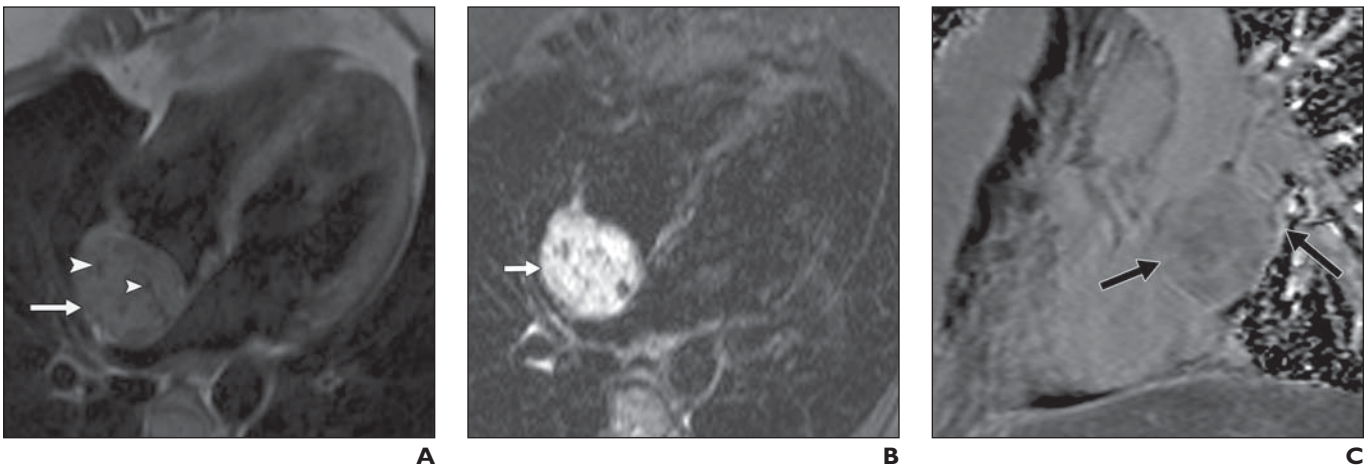

Fig. 16—Pericardial paraganglioma in 37-year-old woman.
A, Axial four-chamber T2-weighted black blood image shows homogeneous intermediate-signal-intensity mass (*arrow*) in right interatrial groove with small areas of flow void within it (*arrowheads*).
B, Axial T2 STIR image shows intensely high-signal-intensity mass (*arrow*) in right interatrial groove.
C, Sagittal phase-contrast inversion recovery gradient-echo sequence shows intense contrast enhancement within mass (*arrows*).

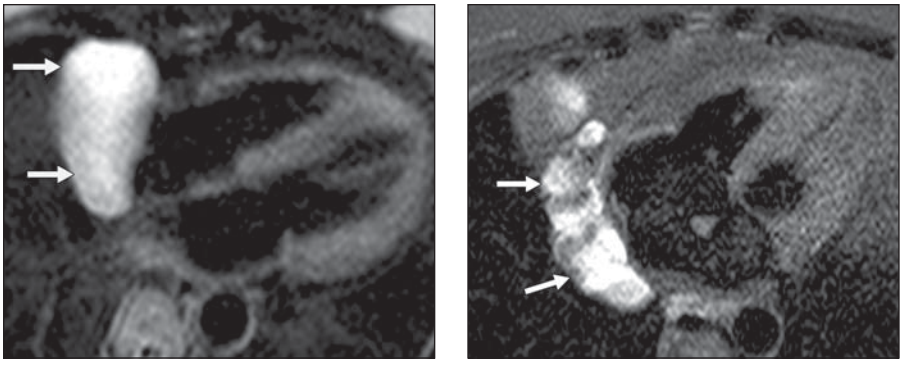

Fig. 17—Pericardial cyst.
A, Axial T2-weighted STIR image of 44-year-old woman shows well-defined lesion with high signal intensity (*arrows*) in right cardiophrenic angle.
B, Axial T2-weighted STIR image of 54-year-old woman shows lobulated cystic lesion with high signal intensity (*arrows*), which is atypical appearance for pericardial cyst.

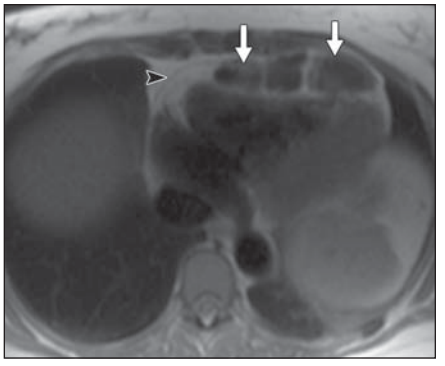

Fig. 18—Bowel in pericardium in 31-year-old man with traumatic diaphragmatic hernia. Axial T2-weighted black blood inversion recovery image shows pericardial defect (*arrows*), which has resulted in herniation of transverse colon into pericardial cavity, is lined by normal-thickness pericardium (*arrowhead*).

FOR YOUR INFORMATION

The data supplement accompanying this Web exclusive article can be viewed from the information box in the upper right corner of the article at: www.ajronline.org.

FOR YOUR INFORMATION

The reader's attention is directed to part 1 accompanying this article, titled "Cardiac MRI: Part 1, Cardiovascular Shunts" which begins on page W603.

FOR YOUR INFORMATION

The Self-Assessment Module accompanying this article can be accessed via www.ajronline.org at the article link labeled "CME/SAM."

The American Roentgen Ray Society is pleased to present these Self-Assessment Modules (SAMs) as part of its commitment to lifelong learning for radiologists. Each SAM is composed of two journal articles along with questions, solutions, and references, which can be found online. Read each article, then answer the accompanying questions and review the solutions online. After submitting your responses, you'll receive immediate feedback and benchmarking data to enable you to assess your results against your peers.

Continuing medical education (CME) and SAM credits are available in each issue of the *AJR* and are ***free to ARRS members. Not a member?*** Call 1-866-940-2777 (from the U.S. or Canada) or 703-729-3353 to speak to an ARRS membership specialist and begin enjoying the benefits of ARRS membership today!